# Cytoplasmic localization of prostate-specific membrane antigen inhibitors may confer advantages for targeted cancer therapies.

Matthias, J.; Engelhardt, J.; Schäfer, M.; Bauder-Wüst, U.; Meyer, P.; Haberkorn, U.; Eder, M.; Kopka, K.; Hell, S.; Eder, A.;

Originally published:

April 2021

**Cancer Research 81(2021)8, 2234-2245**

DOI: https://doi.org/10.1158/0008-5472.CAN-20-1624

# Cytoplasmic localization of prostate-specific membrane antigen inhibitors may confer advantages for targeted cancer therapies

Jessica Matthias[1,2], Johann Engelhardt[1], Martin Schäfer[3], Ulrike Bauder-Wüst[3], Philipp T. Meyer[4,5], Uwe Haberkorn[6,7], Matthias Eder[4,5], Klaus Kopka[3,8,#], Stefan W. Hell[1,9], Ann-Christin Eder[2,3,4,5*]

[1] Department of Optical Nanoscopy, Max Planck Institute for Medical Research, Heidelberg, Germany

[2] Helmholtz International Graduate School, German Cancer Research Center, Heidelberg, Germany

[3] Division of Radiopharmaceutical Chemistry, German Cancer Research Center, Heidelberg, Germany

[4] Department of Nuclear Medicine, University Medical Center Freiburg, Faculty of Medicine, University of Freiburg, Freiburg, Germany

[5] Division of Radiopharmaceutical Development, German Cancer Consortium, partner site Freiburg, Freiburg, Germany and German Cancer Research Center, Heidelberg, Germany

[6] Department of Nuclear Medicine, Heidelberg University Hospital, Heidelberg, Germany

[7] Clinical Cooperation Unit Nuclear Medicine, German Cancer Research Center, Heidelberg, Germany

[8] German Cancer Consortium, Heidelberg, Germany

[9] Department of NanoBiophotonics, Max Planck Institute for Biophysical Chemistry, Göttingen, Germany

[#] current address: Institute of Radiopharmaceutical Cancer Research, Helmholtz-Zentrum Dresden-Rossendorf (HZDR), Dresden, Germany

**Running title**

Cytoplasmic localization of PSMA inhibitors

**Keywords**

Prostate Cancer, Prostate-Specific Membrane Antigen, Dual-Labeled PSMA Inhibitors, Stimulated Emission Depletion Nanoscopy, Theranostics

**Financial support**

ACE and JM received funding from Helmholtz International Graduate School for Cancer Research PhD stipends. ME and KK received support by the VIP+ grant VP00130, Federal Ministry of Education & Research (BMBF), Germany.

***Corresponding author**

Dr. Ann-Christin Eder

University Medical Center Freiburg, Department of Nuclear Medicine

Hugstetter Str. 55

79106 Freiburg im Breisgau

Tel: +49 761 270 63370

Fax: +49 761 270 39300

Email: ann-christin.eder@uniklinik-freiburg.de

**Conflict of interest**

MS, UBW, UH, ME, KK, ACE hold patent rights on dual-labeled PSMA inhibitors. The other authors declare no potential conflicts of interest.

**Additional information**

| | |
|---|---|
| Word count abstract: | 188 |
| Word count main text: | 4963 |
| Number of figures: | 5 |
| Number of tables: | 0 |

## Abstract

Targeted imaging and therapy approaches based on novel prostate-specific membrane antigen (PSMA) inhibitors have fundamentally changed the treatment regimen of prostate cancer. However, the exact mechanism of PSMA inhibitor internalization has not yet been studied and the inhibitors' subcellular fate remained elusive. Here, we have investigated the intracellular distribution of peptidomimetic PSMA inhibitors and of PSMA itself by stimulated emission depletion (STED) nanoscopy applying a novel non-standard live cell staining protocol. Our findings confirm PSMA cluster formation at the cell surface of prostate cancer cells and clathrin-dependent endocytosis of PSMA inhibitors. Following the endosomal pathway, PSMA inhibitors accumulate in prostate cancer cells at clinically relevant time points. Strikingly, in contrast to PSMA itself, PSMA inhibitors were found to eventually distribute homogeneously in the cytoplasm – a molecular condition that promises benefits for treatment, as cytoplasmic and in particular perinuclear enrichment of the radionuclide carriers may better facilitate the radiation-mediated damage of cancerous cells. This study is the first to reveal the subcellular fate of PSMA/PSMA inhibitor complexes at the nanoscale and expected to inspire the development of new approaches in the field of prostate cancer research, diagnostics and therapeutics.

## Statement of significance

This study reveals the subcellular fate of PSMA/PSMA inhibitor complexes close to the molecular level with STED fluorescence nanoscopy. The pioneering insights are of great clinical interest and suggest advantageous targeted therapies.

## Introduction

Prostate cancer is the most common type of cancer in men in western societies and is one of the leading causes of cancer-related mortality (1,2). Among prostate cancer biomarkers for imaging and therapy, the prostate-specific membrane antigen (PSMA) has proven to be an excellent target structure due to (i) its overexpression in prostate cancer, (ii) its absence or low expression rates in healthy tissue (3,4) and (iii) increasing expression rates with tumor aggressiveness, androgen-independence, metastatic disease, and disease recurrence (4-9). PSMA is a transmembrane glycoprotein (100–120 kDa) with an extensive extracellular domain (amino acids 44–750), which undergoes clathrin-mediated internalization upon ligand binding (3,10). A novel MXXXL motif of N-terminal amino acids is formed by the cytoplasmic tail mediating PSMA internalization (11). In colocalization studies with internalized transferrin, PSMA was detected in the recycling endosomal compartment upon tracking with the monoclonal antibody mAB J591, which targets the extracellular domain of PSMA (11,12).

Specific prostate cancer targeting has been successfully achieved by the development of peptidomimetic PSMA inhibitors. Radiolabeling turns these molecules into powerful tools in the diagnosis and therapy of prostate cancer. In diagnostics of all stages, the $^{68}$Ga-labeled PSMA inhibitor Glu-urea-Lys(Ahx)-HBED-CC ([$^{68}$Ga]Ga-PSMA-11) has become the most widely used PET/CT imaging agent (13-19).

Particularly the metastatic, castration-resistant prostate cancer (mCRPCa) represents a major therapeutic challenge as treatment options are still limited. In therapy of mCRPCa, alpha- or beta-emitter radiolabeled PSMA inhibitors (e.g. PSMA-617,

PSMA-I&T) have been introduced as a treatment alternative and first studies have revealed a high efficacy with a favorable safety profile (20,21).

The recently developed dual-modality PSMA inhibitors feature two reporter entities (radioactive and/or fluorescent) enabling both preoperative imaging and subsequent intraoperative (radio- or fluorescence-) guidance (22,23). This approach guarantees the precise detection and resection of malignant tissue to the best possible extent, directly affecting treatment outcome and patient survival. The new class of dual-labeled peptidomimetic PSMA inhibitors paves the way for promising new strategies in the diagnosis and therapy of prostate cancer and several of these molecules are currently in preparation for clinical translation (22,23).

However, the detailed internalization mechanism and the subcellular distribution of PSMA inhibitors are still unknown. In particular, their intracellular fate is of great clinical interest and crucial for obtaining a detailed understanding of the mechanism of action during endoradiotherapy. Stimulated emission depletion (STED) nanoscopy (24,25) provides the spatial resolution to follow PSMA inhibitor trafficking at the nanoscale. Here, we elucidate the internalization mechanism of PSMA inhibitors and determine their subcellular distribution on the molecular level using STED nanoscopy. For visualizing the intracellular distribution patterns of PSMA inhibitors in relation to PSMA, we developed a novel non-standard live cell immunofluorescence (IF) staining protocol. To the best of our knowledge, this study is the first to investigate and reveal the subcellular fate of PSMA/PSMA inhibitor complexes.

## Material and Methods

### *Synthesis, radiolabeling and determination of fluorescence properties*

The STED-compatible dual-labeled PSMA inhibitors Glu-urea-Lys-HBED-CC-$PEG_2$-STAR RED and Glu-urea-Lys-HBED-CC-$PEG_2$-STAR 635P (hereinafter referred to as Glu-urea-Lys-HBED-CC-<dye> for <dye> conjugates) were synthesized according to previous procedures (22). Radioisotope labeling with $^{68}$Ga and determination of fluorescence properties were conducted according to previously established protocols. Details on synthesis, radiolabeling and fluorescence spectroscopy are provided in Supplementary Methods.

### *Cell culture*

For cultivation of PSMA-positive androgen-sensitive human prostate adenocarcinoma cells (LNCaP, ATCC CRL-1740, RRID:CVCL_1379, high PSMA expression; 22Rv1, ATCC CRL-2505, RRID: CVCL_1045, moderate/heterogeneous PSMA expression) and PSMA-negative androgen non-reliant human prostate adenocarcinoma cells (PC-3, ATCC CRL-1435, RRID**:**CVCL_0035), RPMI medium was enriched with 10% FCS and 2 mmol/L L-glutamine (all from PAA). Cells were grown at 37°C in humidified air with 5% $CO_2$ and were harvested using trypsin-ethylenediaminetetraacetic acid (trypsin-EDTA, 0.25% trypsin, 0.02% EDTA, Gibco, Cat#25200056; <20 passages between thawing and experimental use). Cell line authentication and mycoplasma testing is regularly performed. Authentication of the LNCaP and PC-3 cell lines was confirmed on 03/06/2020. The 22Rv1 cell line was directly obtained from ATCC (purchased on 05/29/2020; Lot: 2215512).

Cell binding and internalization experiments were performed as previously described (13). Potential cytotoxicity was assessed by analyzing the duration and frequency of cell division via holographic time-lapse imaging with a HoloMonitor® M4 cytometer (PHI AB). Details to cell binding, internalization and cytotoxicity experiments are provided in Supplementary Methods.

### *Biodistribution, PET imaging and cryosectioning studies*

Biodistribution and PET imaging studies in LNCaP- and PC-3-tumor xenograft mice were performed according to established protocols (22). For cryosectioning, tissue was directly frozen 1 h after tracer injection (details in Supplementary Methods). All experiments complied with the current laws of the Federal Republic of Germany and were conducted according to German Animal Welfare guidelines and ARRIVE guidelines. The experiments were approved by the regional authorities *Regierungspräsidium Karlsruhe* and *Freiburg* (approval numbers G158/15, G18/04).

### *STED and confocal microscopy*

All confocal and STED data were acquired with a custom-built STED system close to the one published by Gorlitz et al. (26) (details in Supplementary Methods).

For assessing the time and concentration dependence of PSMA inhibitor internalization, cells were incubated with 50/100/250/500 nM Glu-urea-Lys-HBED-CC-STAR RED in RPMI for 5/15/30/45 min at room temperature. To verify specific uptake, cells were co-incubated with 2-PMPA (500 µM). Additionally, potential internalization of free dye was tested by incubating cells with STAR RED and STAR 635P carboxylic acid (Abberior, Cat#STRED-0001, Cat#ST635P-0001) for 1 h

at 37°C. After fixation with paraformaldehyde (2% PFA in PBS) for 10 min, the samples were mounted with ProLong Diamond Antifade Mountant containing DAPI (Thermo Fisher Scientific, Cat#P36966).

For live cell imaging and colocalization experiments, a novel non-standard live cell staining protocol exploited the blocking effect of low temperatures on PSMA internalization without impairing cell health. Briefly, cells were immunolabeled against PSMA and/or incubated with dual-labeled PSMA inhibitors on ice to specifically target the entire cell membrane-bound PSMA fraction. Internalization of the antibody/PSMA/PSMA inhibitor complex was triggered by temperature increase. For PSMA IF, a monoclonal anti-PSMA antibody (1:50, mouse IgG1, clone 107-1A4, Sigma-Aldrich, Cat#SAB4200257, RRID:AB_11129838) and a STAR 600-labeled goat anti-mouse-IgG antibody (1:50, Abberior, Cat#2-0002-010-5) were used. For colocalization experiments with clathrin, LNCaP cells were transiently transfected with the fusion construct SNAP-tag/clathrin light chain (SNAP-CLC) and stained with the live dye 610CP-BG (27,28). Clathrin-mediated endocytosis was blocked via co-incubation with 30 µM Pitstop 2 (Sigma-Aldrich, Cat#SML1169). For endosomal colocalization experiments, LysoTracker™ Green DND-26 (Thermo Fisher Scientific, Cat#L7526) or SiR-lysosome (SPIROCHROME, Cat#SC012) were used. Details on microscopy sample preparation and colocalization experiments are provided in Supplementary Methods.

Background correction was done by subtracting at most 10% of the maximum fluorescence signal. Linear deconvolution (Wiener filter) was applied with a Lorentzian PSF (FWHM STED PSF 60 nm, FWHM confocal PSF 200 nm) and only to the extent that data are smoothed and noise is reduced but resolution is not

increased. Detailed information on microscopy data analysis are provided in Supplementary Methods.

***Flow cytometry studies on PSMA binding affinity and pH dependence***

The binding affinity of Glu-urea-Lys-HBED-CC-STAR RED and -STAR 635P (0.0/0.5/1.0/2.5/5.0/10/25/50/100/500 nM) to PSMA on LNCaP and 22Rv1 cells was determined as the mean effective concentration ($EC_{50}$) by flow cytometry (BD FACS Canto II Flow Cytometer, BD Biosciences). To demonstrate the specificity of the binding, all conjugates in concentrations of 0.5/5.0/50 nM were additionally co-incubated with 500 µM 2-PMPA. The pH dependence of the binding was analyzed for Glu-urea-Lys-HBED-CC-STAR RED, -STAR 635P and the antibody complex (primary antibody: monoclonal anti-PSMA, mouse IgG1, clone 107-1A4, Sigma-Aldrich, Cat#SAB4200257, RRID:AB_11129838; secondary antibodies: STAR 600- or STAR RED-labeled goat anti-mouse-IgG, Abberior, Cat#2-0002-010-5 or Cat#2-0002-011-2, RRID:AB_2810982). Details on the flow cytometry studies are provided in Supplementary Methods.

***Statistical aspects and data presentation***

Experiments were performed at least in triplicate. Quantitative data in text are expressed as mean ± standard deviation (SD). Bar plots depict the mean ± SD of the measurements for replicate experiments. Box plots indicate the interquartile range (box), the outer-most data points falling within 1.5× interquartile range (whiskers), the median (center line) and the mean (triangle) of the measurements for replicate experiments. If applicable, means were compared using Student´s t test (GraphPad Prism Version 7, GraphPad Software, Inc.). P-values $< 0.05$ were considered statistically significant.

228

## Results

### *STED-Compatible Dual-Labeled PSMA Inhibitors Feature High PSMA Affinity and Specific Internalization Properties In Vitro.*

STED-compatible dual-labeled PSMA inhibitors were derived from Glu-urea-Lys-HBED-CC-$PEG_2$-IRDye800CW, as the latter preclinically performs comparably to clinically established molecules (e.g. PSMA-11 or PSMA-617) (13,22,29,30). The analytical data of the final products Glu-urea-Lys-HBED-CC-$PEG_2$-STAR RED and Glu-urea-Lys-HBED-CC-$PEG_2$-STAR 635P are summarized Table S1, their structures are shown in Fig. 1A, and their fluorescence spectra are displayed in Fig. S1.

Incubation of LNCaP (high PSMA expression) and 22Rv1 (moderate/heterogeneous PSMA expression) cells with $^{68}$Ga-labeled Glu-urea-Lys-HBED-CC-STAR RED and -STAR 635P resulted in significant and specific binding to PSMA with affinities in the low nanomolar range. Additionally, both conjugates specifically internalized (Table S2). The pronounced difference in PSMA expression levels (31) accounts for the reduced signal of 22Rv1 cells. This trend is likewise reflected in all following fluorescence imaging experiments.

To ascertain and elaborate on the radioactively determined *in vitro* data, cell binding and internalization was investigated in confocal microscopy experiments (Fig. 1B). All subsequent fluorescence microscopy data were acquired with Glu-urea-Lys-HBED-CC-STAR RED, as this conjugate displayed superior photostability and contrast in the fluorescence imaging experiments. Confocal imaging detected an increasing accumulation of Glu-urea-Lys-HBED-CC-STAR RED in PSMA-positive cells independent of its concentration over time (Fig. S2). A blocking effect was not detected for the tested concentration range (50 nM to 500 nM). Blocking studies in

the presence of 500 µM 2-PMPA, internalization experiments with the free Abberior dyes STAR RED and STAR 635P and with PSMA-negative PC-3 cells proved the specificity of PSMA binding and internalization (Fig. S3A-D).

For confocal time-lapse experiments, LNCaP cells were incubated with Glu-urea-Lys-HBED-CC-STAR RED for 20 min on ice to prevent premature internalization, subsequently washed and immediately imaged. Over a period of 120 min, steady internalization was observed (Fig. S3E and F, Movie S1). No morphological changes or other signs of impaired cell viability were detected during the experiment. To rigorously exclude cytotoxicity by the PSMA inhibitor, the frequency and duration of cell division was assessed via holographic time-lapse imaging. Cell proliferation was followed in the presence of either Glu-urea-Lys-HBED-CC-STAR RED or -STAR 635P for 48 h and was compared to the proliferation of untreated cells. The data show no evidence of cytotoxicity but a slightly accelerated LNCaP cell proliferation in the presence of PSMA inhibitors (Fig. 1C and D, Fig. S4, Fig. S5, Table S3, Movie S2-S4).

***LNCaP Xenograft Tumors in Mice are Specifically Targeted by STED-Compatible Dual-Labeled PSMA Inhibitors.***

The ability of Glu-urea-Lys-HBED-CC-STAR RED and -STAR 635P to specifically target PSMA *in vivo* was evaluated in biodistribution studies at 1 h post injection (p.i.). Both conjugates performed similarly in a PSMA-expressing LNCaP tumor mouse xenograft model with a high tumor uptake of around 5 %ID/g and a favorable organ distribution profile comparable to PSMA-11, the reference compound without dye (30) (Fig. 2A, Table S4). Confocal imaging of tumor and muscle tissue cryosections confirmed a PSMA-specific uptake and revealed a homogenous

subcellular distribution pattern throughout the tumor cells already 1 h p.i. (Fig. 2B). The specificity of the *in vivo* tumor uptake of Glu-urea-Lys-HBED-CC-STAR RED was further proven with PSMA-negative PC-3 tumor xenografts. The uptake in PSMA-negative tumor tissue was comparable to the uptake in muscle tissue (Table S5).

Additionally, small-animal PET imaging was performed with $^{68}$Ga-labeled Glu-urea-Lys-HBED-CC-STAR RED. Selective tumor uptake in the LNCaP xenograft model accompanied by rapid clearance from off-target tissue resulted in a high imaging contrast at early time points. In PSMA-negative PC-3 xenografts, no measurable uptake of the conjugate was observed during the experiment, demonstrating high PSMA specificity (Fig. 2C). The corresponding time activity curves showed rapid clearance from muscle, liver and heart tissues, but continuous accumulation of the conjugate in kidneys and bladder confirming the renal elimination (Fig. 2D).

***Clathrin Mediates the Internalization of PSMA Inhibitors after PSMA Binding.***

To resolve details of the PSMA distribution in the cell membrane, Glu-urea-Lys-HBED-CC-STAR RED bound PSMA was imaged with STED nanoscopy. A heterogeneous distribution of the fluorescence signal along the cell membrane was observed, suggesting areas of higher and lower PSMA density, which could not be visualized with confocal imaging. Within the patches of high PSMA density, round to oval-shaped PSMA clusters of various sizes were detected (Fig. 3A, Fig. S6A).

After short internalization times, the PSMA inhibitor signal was localized to the membrane of cytoplasmic vesicles. While confocal imaging visualized the vesicles as blurred diffraction-limited spots, STED imaging enabled the nanometer resolution of

defined, hollow, spherical structures (Fig. 3B and C). Heterogeneous vesicle distribution was observed with regions of higher and lower vesicle density. While the nucleus always remained free of any Glu-urea-Lys-HBED-CC-STAR RED signal, the overall concentration of vesicles in cellular filopodia increased particularly (Fig. 3D). Line profiles of vesicles derived from raw confocal and STED data confirm the improvement in resolution gained by STED. The full width half maxima (FWHMs) of the Lorentzian fits suggest a spatial resolution significantly below the diffraction limit (Fig. 3C, Fig. S6B and C; for postprocessing of STED data refer to Fig. S7).

Live LNCaP cell confocal colocalization experiments between Glu-urea-Lys-HBED-CC-STAR RED and SNAP-tagged CLC labeled with 610CP (27,28) showed a significant signal overlap for early time points that decreased with progressing internalization time (Fig. 3E, Fig. S8A). The Pearson's correlation coefficient (PCC) (32) dropped significantly within the first 15 min of internalization, suggesting clathrin-mediated uptake with rapid clathrin uncoating after internalization (Fig. 3F, Table S6), which enabled the fusion with early endosomes and thus vesicle growth (33,34). Co-incubation with the clathrin inhibitor Pitstop 2 confirmed clathrin-dependent PSMA inhibitor internalization (Fig. S8B and C).

As clathrin coated vesicles (CCVs) feature a well-defined diameter, the diameter of endocytic vesicles is an indicator for the degree of progress along the endocytic pathway. It was analyzed by fitting a two-dimensional ring function to the fluorescence signal (Fig. S6D). The average diameter does not differ significantly within the first hour of internalization. The large SDs indicate a broad spread of diameter in the overall vesicle population, especially for later times (Fig. 3G, Table S7). These values are in the range of but, especially for LNCaP cells, always larger than the size of CCVs as published in the literature (35,36).

***PSMA Inhibitors Distribute Homogeneously in the Cytoplasm Over Time.***

For assessing the extent and duration of colocalization of the PSMA inhibitors with PSMA during and after the internalization process, incubation with Glu-urea-Lys-HBED-CC-STAR RED was combined with indirect immunolabeling of PSMA with the Abberior dye STAR 600 in a novel non-standard live cell staining protocol. To avoid premature PSMA internalization, living cells were stained on ice and internalization times were well defined by subsequent incubation at 37°C (Fig. 4A, Fig. S9). The PSMA inhibitor and the primary/secondary antibody complex were both internalized without any evidence for mutual blocking effects. The intracellular distribution of the PSMA inhibitor and PSMA was visualized for different internalization times by STED (LNCaP) and confocal (22Rv1) microscopy.

Due to biological heterogeneity, we rather state qualitative trends than quantitative numbers. Colocalization trends can be illustrated in pixel fluorograms (37) (hereinafter referred to as fluorograms; for details, see Supplementary Methods). For visualizing the time-dependent changes in the colocalization of PSMA inhibitor and PSMA, we subdivided the fluorograms of all dual color STED/confocal images in three defined sections separating (i) the PSMA antibody signal only (top section), (ii) the colocalizing signal (middle section) and (iii) the PSMA inhibitor signal only (bottom section). The background (quarter circle in bottom left corner) was set to the average intensity of Glu-urea-Lys-HBED-CC-STAR RED after 24 h of internalization (Fig. 4B).

For short internalization times, the PSMA inhibitor signal (red) and the PSMA antibody signal (cyan) strongly colocalized in one fraction (white) falling into the middle section of the fluorogram representing specific binding of the PSMA inhibitor to PSMA in the plasma and vesicle membrane (Fig. 4C, Fig. S10). The corresponding PCC peaked at 30 min with r(LNCaP)=0.65±0.08 (*N*=9) and r(22Rv1)=0.70±0.06 (*N*=15). During the first hour of internalization, continuing colocalization of the signals at the membrane of cytoplasmic vesicles was detected with an average PCC of r(LNCaP)=0.54±0.09 (*N*=43) and r(22Rv1)=0.65±0.07 (*N*=56).

However, around 45 min, the cyan fraction (PSMA antibody) started to increase significantly in the fluorogram's top section and the red fraction (PSMA inhibitor) started to slowly vanish into the background. Over time, the relative intensities of both signals in the foreground of the middle section of the fluorogram, and thus the colocalizing fraction, significantly declined. The relative intensity of the PSMA inhibitor in the entire foreground of the fluorogram (all three sections taken together) significantly decreased while it increased in the entire background. However, the relative intensity of PSMA changed neither in the entire foreground nor in the entire background (Fig. 4C, Fig. S10, Fig. S11A-E).

These trends illustrate the gradual release of the PSMA inhibitor from PSMA. The PSMA inhibitor signal initially distributed homogeneously in the vesicles (Fig. 4D*)* and finally dispersed in the cytoplasm after >3 h of internalization (Fig. 4E and F, Fig. S11F, Table S8). At these times, the PSMA antibody signal was still detected at the vesicle membrane and additionally in dotted patches at the cell membrane, presumably representing recycled PSMA (see next subsection).

At later time points (6 h, 24 h), no significant further changes of the signal distribution were observed (Fig. S11A-F) and the colocalization between PSMA inhibitor and PSMA was significantly reduced with an average PCC of r(LNCaP)=0.25±0.12 (*N*=18) and r(22Rv1)=29±0.15 (*N*=21). Photobleaching was found to be negligible as the ratio of the integrated fluorescence intensities did not drastically change over time with an average of 1.17±0.35 (LNCaP *N*=57, PSMA to PSMA inhibitor). Dye-dependent effects could be excluded by substantiating the results of Glu-urea-Lys-HBED-CC-STAR RED with Glu-urea-Lys-HBED-CC-STAR 635P and the results of PSMA STAR 600 IF with PSMA STAR RED IF (Fig. S11G and H).

***PSMA Is Recycled in the Endosomal Compartment.***

To obtain more information on the PSMA recycling pathway, endosomal colocalization experiments were carried out. Living cells were immunolabeled for cell membrane-bound PSMA on ice to prevent premature PSMA internalization. Subsequently, internalization was triggered by incubation at 37°C. After different internalization times, endosomal colocalization was assessed during live cell confocal imaging experiments by staining with LysoTracker™ Green DND-26, which is selective for both lysosomes and endosomes. With progressing internalization time, the PSMA signal increasingly overlapped with the endosomal signal and the respective PCC significantly climbed (Fig. 5A and B, Table S9), suggesting endosomal recycling of PSMA. Non-colocalizing LysoTracker signal was additionally detected due to unlabeled PSMA and non-PSMA-carrying lysosomes (Movie S5). Co-incubation with 2-PMPA, Glu-urea-Lys-HBED-CC-STAR RED or -STAR 635P did not significantly affect the degree of colocalization (Table S9). PSMA recycling was further supported by the occurrence of clustered PSMA antibody signals at the cell

membrane not colocalizing with PSMA inhibitor in confocal and STED imaging experiments after 45 min of internalization (Fig. 5C).

The results were confirmed in live confocal and live STED colocalization experiments by co-staining with SiR-lysosome, which also targets both lysosomes and endosomes (Fig. S12A, Movie S5). To exclude phototoxic influence, low light intensity confocal times-series of lysosomal dynamics were recorded after STED imaging. No qualitative difference in lysosomal movement was observed compared to control cells not exposed to high STED laser intensities (Movie S6 and S7).

***PSMA Binding is pH Dependent.***

The homogeneous cytoplasmic distribution of Glu-urea-Lys-HBED-CC-STAR RED for internalization times >3 h suggested a separation of the PSMA/PSMA inhibitor complex in the endosomes by decreasing pH. To test this hypothesis, the pH dependence of the binding properties of the PSMA antibody and the PSMA inhibitor to PSMA on LNCaP cells were assessed. In flow cytometry studies, the fractions bound at different physiologically relevant pH values in percent of the fraction bound at pH 7.0 were measured via the detected fluorescence signal of the PSMA inhibitors or the secondary antibodies. The binding of the antibody complexes (primary monoclonal anti-PSMA antibody decorated with secondary antibody conjugated to Abberior STAR 600 or Abberior STAR RED) to PSMA was not significantly affected up to an acidic pH of 4.6. In contrast, the binding of Glu-urea-Lys-HBED-CC-STAR RED and -STAR 635P to PSMA was drastically reduced with increasing acidity (Fig. 5D, Tables S10 and S11). Temperature and/or pH dependent fluorophore degradation of the PSMA inhibitors could be excluded (Fig. S12B and C).

## Discussion

PSMA-targeted imaging and therapy has refashioned the diagnosis and the treatment of prostate cancer patients over the last years (14-16,19). In particular, endoradiotherapy with alpha- or beta-emitter radiolabeled PSMA inhibitors offers a promising treatment approach for late stage mCRPCa patients beyond established treatment options (20,21).

With the development of dual-labeled PSMA inhibitors, an additional imaging modality has been successfully introduced to the clinical routine (22,23,38). Besides intraoperative fluorescence-guided surgery, the additional fluorescence property enables intracellular tracking of the dual-labeled inhibitor, making it a perfect model compound for analyzing the subcellular fate of peptidomimetic PSMA inhibitors at the nanoscale. To the best of our knowledge, the detailed subcellular fate of PSMA/ PSMA inhibitor complexes for peptidomimetic PSMA inhibitors has not been investigated with fluorescence nanoscopy so far.

All existing knowledge on the mechanism of internalization and the intracellular distribution of PSMA is solely based on diffraction-limited confocal microscopy studies (11,12). The herein achieved spatial resolution is indeed sufficient to follow the coarse localization of PSMA and its inhibitors inside cells over time. However, to precisely investigate localization subtleties (e.g. cluster substructures) and to elucidate in detail the subcellular fate of PSMA and PSMA inhibitor (e.g. molecular colocalization), STED nanoscopy is the method of choice, as it combines the required spatial resolution with inherently coaligned fluorescence imaging channels (excitation multiplexed, one STED donut) (39).

Since this nanoscopy technique places special demands on the fluorophores used (40), we synthesized dual-labeled PSMA inhibitors based on PSMA-11 equipped with the STED-compatible Abberior dyes STAR RED and STAR 635P. Both conjugates exhibited high PSMA-specific binding affinities, specifically internalized fractions, specific tumor uptake in PSMA-positive lesions and high tumor-to-background ratios at early time points comparable to the parental structure (22) and reference compounds without dye (13,29). Hence, the additional fluorescence moiety does not affect the main characteristics of our conjugates (e.g. pharmacokinetic properties, tumor accumulation), making them suitable for mimicking clinically used PSMA inhibitors to study their intracellular fate with STED nanoscopy.

Confocal and STED imaging as a function of time permitted the visualization of the intracellular distribution of PSMA and of our PSMA inhibitors in PSMA-expressing LNCaP and 22Rv1 cells. The data revealed an increase of the internalized PSMA inhibitor fraction over time, independently of the concentrations tested. These results support the radioactively determined *in vitro* data acquired with the $^{68}$Ga-labeled PSMA inhibitors in cell binding and internalization studies.

Long-term PSMA inhibitor internalization experiments using confocal and STED imaging indicate enrichment in cells. These findings are in line with the *in vivo* time course of tumor accumulation, which agrees with our observations of a long-term accumulation of our PSMA inhibitors in prostate cancer tumor cells with a high signal-to-background ratio. Non-specific signal of unbound inhibitors decreased over time, while the signal of the specifically internalized fraction remained. Targeting of non-tumor tissue was very limited, but even if off-target internalization were to occur, our holographic cytometry data does not indicate cytotoxic effects by the non-radiolabeled PSMA inhibitors.

STED nanoscopy allowed the visualization of structural subtleties of the cell membrane-bound PSMA fraction (assessed with both PSMA IF and PSMA inhibitor). The PSMA signal was not homogeneously distributed along the cell membrane, but rather spread into patches of oval- to round-shaped signals of different sizes, both before internalization and after PSMA recycling. We assume that these individual signals consist of varying numbers of PSMA molecules grouped in clusters at the cell membrane. PSMA clustering at the cell surface was previously suggested based on data of biochemical assays, in which it was artificially induced with antibodies. PSMA clustering is crucial not only for PSMA activation and its subsequent internalization, but also for many downstream signalling pathways directly or indirectly affecting cell proliferation (41-43) potentially explaining the slightly accelerated LNCaP division frequency and duration we observed.

With STED nanoscopy, we visualized PSMA clustering at the cell surface for the first time, induced either by antibodies or by our PSMA inhibitors. During the LysoTracker colocalization experiments, we did not observe significant differences in endosomal colocalization in the presence or absence of our PSMA inhibitors, as PSMA clustering, activation and internalization was in any case induced by our PSMA IF labeling approach.

During the early phase of the internalization process, cytoplasmic vesicle formation was observed. Live cell colocalization experiments suggest that the PSMA-specific internalization of peptidomimetic PSMA inhibitors is mediated via clathrin-dependent endocytosis. As resolved by STED imaging, the average vesicle diameter is more than twice the value for CCVs found in literature (35,36) but the large SD indicates a very heterogeneous vesicle population in our samples. The FWHMs of selected vesicle line profiles suggest a resolution good enough to resolve vesicles with

approx. 100 nm in diameter. Thus, we assume that we mostly detected early endosomes, as CCVs quickly uncoat and fuse to become early endosomes with diameters larger than CCVs. We could indeed confirm that PSMA itself passes the endosomal pathway to be either degraded in lysosomes or recycled back to the cell surface as previously described (10,11).

Furthermore, we developed a novel non-standard live cell IF staining protocol to visualize the intracellular distribution of our PSMA inhibitors in relation to PSMA. In general, antibody staining is limited to fixed cells as antibodies are not cell membrane permeable. Here, we exploited the fact that PSMA internalization can be blocked by low temperature without impairing cell health. Thus, the entire cell membrane-bound PSMA fraction could be labeled by incubating the cells on ice. A subsequent temperature increase triggered the internalization of the antibody/PSMA/PSMA inhibitor complex (Fig. S9). While indirect IF provides strong signal amplification, our PSMA inhibitors add only one fluorophore per PSMA molecule. Despite this difference in fluorophore stoichiometry, the brightness and signal-to-noise ratio of the PSMA inhibitor signal is only slightly reduced to the immunolabeled PSMA signal.

Interestingly, peptidomimetic PSMA inhibitors appear to distribute fundamentally differently on the subcellular level than PSMA antibodies used for prostate cancer immunotherapy. For short internalization times, strong colocalization was observed between PSMA and our PSMA inhibitors, but it decreased over time and eventually vanished at later time points. The PSMA/PSMA inhibitor complex dissociates during the PSMA recycling process in the endosomal compartment allowing the PSMA inhibitors initially to distribute in the endosomes but to disperse gradually homogeneously in the cytoplasm without binding to other structures. Immunolabeled PSMA remained in the vesicle membrane, eventually to be recycled back to the cell

membrane. Rajasekaran *et al.* previously reported on internalization and vesicle formation of antibody-targeted PSMA after 2 h of incubation (11). Our findings match these results but additionally visualize PSMA localization at later time points up to 24 h.

A dye-dependent effect could be excluded by interchanging the fluorescent labels for immunolabeled PSMA and PSMA inhibitor. It could additionally be shown that the spectral properties of our PSMA inhibitors were not sensitive to acidic pH or elevated temperature and, as unnatural inhibitors of PSMA, our conjugates are presumably intrinsically inert to lysosomal digestion.

Remarkably, significant differences in the binding affinity to PSMA at acidic pH were detected between the antibody and PSMA inhibitor. The interaction between PSMA and PSMA inhibitor decreased drastically at acidic pH, whereas binding of the anti-PSMA antibody/secondary antibody complex remained unaffected. The difference in pH sensitivity of PSMA binding is one plausible explanation for the fundamentally different intracellular distributions observed for the antibody and PSMA inhibitor. With decreasing endosomal pH, the PSMA binding affinity of the PSMA inhibitors is reduced, shifting the equilibrium between bound and unbound PSMA inhibitor towards the unbound state. We now speculate that, at endosomal pH, the acidic moieties of PSMA inhibitors are mostly protonated, allowing for endosomal escape and cytoplasmic dispersion. Following this hypothesis, unbound PSMA inhibitor would be continuously removed from the PSMA bound/unbound collective inside the endosomes. By pushing the position of the equilibrium further towards the unbound state, eventually, the entire PSMA inhibitor population would be located inside the cytoplasm, a process simply driven by entropy. Finally, the cytoplasm's neutral pH is assumed to trap the PSMA inhibitors inside the cell by deprotonating their acidic

moieties, thereby restoring the molecules' membrane impermeability. However, further studies on externalization and membrane permeability need to confirm this hypothesis.

The performance of prostate cancer targeting inhibitors in diagnostics and therapy highly depends on their cell binding and internalization properties as well as on their subcellular localization. This study describes the intracellular distribution of PSMA and peptidomimetic PSMA inhibitors at the nanometer scale for the first time. STED fluorescence nanoscopy allows insights into the internalization and precise localization of both PSMA inhibitors and of PSMA itself at clinically relevant time points. As observed in this study, strong and specific internalization in combination with a long retention allows the inhibitors' enrichment in the target cells over time affording high imaging contrasts while sparing healthy tissue and preventing off-target tissue effects. The striking difference between the PSMA antibodies' and the PSMA inhibitors' subcellular fate will potentially have significant impact on the therapeutic efficiency of the peptidomimetic inhibitors. The homogeneous dispersion of PSMA inhibitors in prostate cancer cells after internalization, which we have demonstrated here for the first time, is of particular interest in endoradiotherapy, for which this dispersed cytoplasmic distribution potentially leads to beneficial effects. Intracellular accumulation and localization in nuclear proximity may allow a more target-oriented application of effectively higher local radiation doses – especially with high linear energy transfer alpha particles - resulting in potent DNA damage and subsequent apoptosis.

We expect our results to fuel further ligand development, not only in the field of prostate cancer. Our findings will hopefully boost the development of refined and/or

571 new targeting strategies for diagnostic and therapeutic approaches in prostate cancer
572 and other human cancer treatment.

## Acknowledgments

We acknowledge funding from Helmholtz International Graduate School for Cancer Research PhD stipends for ACE and JM and support by the VIP+ grant VP00130, Federal Ministry of Education& Research (BMBF), Germany. We thank Karin Leotta, Ursula Schierbaum and Mareike Roscher for support in biodistribution and small-animal imaging studies, Martin Seefeld for providing access to UV/Vis and fluorescence spectrophotometers, Alexey Butkevich and Vladimir Belov for providing the fluorescent live dye 610CP-BG, Francesca Bottanelli for providing the SNAP-CLC construct, Steffen J. Sahl and Jade Cottam Jones for helpful discussions, and Rifka Vlijm for support in data analysis.

## References


1. Ferlay J, Steliarova-Foucher E, Lortet-Tieulent J, Rosso S, Coebergh JW, Comber H*, et al.* Cancer incidence and mortality patterns in Europe: estimates for 40 countries in 2012. *Eur J Cancer* **2013**;49:1374-403.
2. Siegel RL, Miller KD, Jemal A. Cancer statistics, 2019. *CA Cancer J Clin* **2019**;69:7-34.
3. Ghosh A, Heston WD. Tumor target prostate specific membrane antigen (PSMA) and its regulation in prostate cancer. *J Cell Biochem* **2004**;91:528-39.
4. Silver DA, Pellicer I, Fair WR, Heston WD, Cordon-Cardo C. Prostate-specific membrane antigen expression in normal and malignant human tissues. *Clin Cancer Res* **1997**;3:81-5.
5. Wright GL, Jr., Haley C, Beckett ML, Schellhammer PF. Expression of prostate-specific membrane antigen in normal, benign, and malignant prostate tissues. *Urologic oncology* **1995**;1:18-28.
6. Sweat SD, Pacelli A, Murphy GP, Bostwick DG. Prostate-specific membrane antigen expression is greatest in prostate adenocarcinoma and lymph node metastases. *Urology* **1998**;52:637-40.
7. Mhawech-Fauceglia P, Zhang S, Terracciano L, Sauter G, Chadhuri A, Herrmann FR*, et al.* Prostate-specific membrane antigen (PSMA) protein expression in normal and neoplastic tissues and its sensitivity and specificity in prostate adenocarcinoma: an immunohistochemical study using mutiple tumour tissue microarray technique. *Histopathology* **2007**;50:472-83.
8. Minner S, Wittmer C, Graefen M, Salomon G, Steuber T, Haese A*, et al.* High level PSMA expression is associated with early psa recurrence in surgically treated prostate cancer. *Prostate* **2011**;71:281-8.
9. Ross JS, Sheehan CE, Fisher HA, Kaufman RP, Jr., Kaur P, Gray K*, et al.* Correlation of primary tumor prostate-specific membrane antigen expression with disease recurrence in prostate cancer. *Clin Cancer Res* **2003**;9:6357-62.
10. Liu H, Rajasekaran AK, Moy P, Xia Y, Kim S, Navarro V*, et al.* Constitutive and antibody-induced internalization of prostate-specific membrane antigen. *Cancer Res* **1998**;58:4055-60.
11. Rajasekaran SA, Anilkumar G, Oshima E, Bowie JU, Liu H, Heston W*, et al.* A novel cytoplasmic tail MXXXL motif mediates the internalization of prostate-specific membrane antigen. *Mol Biol Cell* **2003**;14:4835-45.
12. Smith-Jones PM, Vallabahajosula S, Goldsmith SJ, Navarro V, Hunter CJ, Bastidas D*, et al.* In vitro characterization of radiolabeled monoclonal antibodies specific for the extracellular domain of prostate-specific membrane antigen. *Cancer Res* **2000**;60:5237-43.
13. Eder M, Schafer M, Bauder-Wust U, Hull WE, Wangler C, Mier W*, et al.* 68Ga-complex lipophilicity and the targeting property of a urea-based PSMA inhibitor for PET imaging. *Bioconjug Chem* **2012**;23:688-97.
14. Zamboglou C, Drendel V, Jilg CA, Rischke HC, Beck TI, Schultze-Seemann W*, et al.* Comparison of (68)Ga-HBED-CC PSMA-PET/CT and multiparametric MRI for gross tumour volume detection in patients with primary prostate cancer based on slice by slice comparison with histopathology. *Theranostics* **2017**;7:228-37.
15. Maurer T, Gschwend JE, Rauscher I, Souvatzoglou M, Haller B, Weirich G*, et al.* Diagnostic Efficacy of (68)Gallium-PSMA Positron Emission Tomography Compared to Conventional Imaging for Lymph Node Staging of 130

Consecutive Patients with Intermediate to High Risk Prostate Cancer. *J Urol* **2016**;195:1436-43.
16. Pyka T, Okamoto S, Dahlbender M, Tauber R, Retz M, Heck M*, et al.* Comparison of bone scintigraphy and (68)Ga-PSMA PET for skeletal staging in prostate cancer. *Eur J Nucl Med Mol Imaging* **2016**;43:2114-21.
17. Herlemann A, Wenter V, Kretschmer A, Thierfelder KM, Bartenstein P, Faber C*, et al.* (68)Ga-PSMA Positron Emission Tomography/Computed Tomography Provides Accurate Staging of Lymph Node Regions Prior to Lymph Node Dissection in Patients with Prostate Cancer. *Eur Urol* **2016**;70:553-7.
18. Perera M, Papa N, Roberts M, Williams M, Udovicich C, Vela I*, et al.* Gallium-68 Prostate-specific Membrane Antigen Positron Emission Tomography in Advanced Prostate Cancer-Updated Diagnostic Utility, Sensitivity, Specificity, and Distribution of Prostate-specific Membrane Antigen-avid Lesions: A Systematic Review and Meta-analysis. *Eur Urol* **2019**.
19. Hope TA, Aggarwal R, Chee B, Tao D, Greene KL, Cooperberg MR*, et al.* Impact of (68)Ga-PSMA-11 PET on Management in Patients with Biochemically Recurrent Prostate Cancer. *J Nucl Med* **2017**;58:1956-61.
20. Rahbar K, Ahmadzadehfar H, Kratochwil C, Haberkorn U, Schafers M, Essler M*, et al.* German Multicenter Study Investigating 177Lu-PSMA-617 Radioligand Therapy in Advanced Prostate Cancer Patients. *J Nucl Med* **2017**;58:85-90.
21. Baum RP, Kulkarni HR, Schuchardt C, Singh A, Wirtz M, Wiessalla S*, et al.* 177Lu-Labeled Prostate-Specific Membrane Antigen Radioligand Therapy of Metastatic Castration-Resistant Prostate Cancer: Safety and Efficacy. *J Nucl Med* **2016**;57:1006-13.
22. Baranski AC, Schafer M, Bauder-Wust U, Roscher M, Schmidt J, Stenau E*, et al.* PSMA-11-Derived Dual-Labeled PSMA Inhibitors for Preoperative PET Imaging and Precise Fluorescence-Guided Surgery of Prostate Cancer. *J Nucl Med* **2018**;59:639-45.
23. Schottelius M, Wurzer A, Wissmiller K, Beck R, Koch M, Gorpas D*, et al.* Synthesis and Preclinical Characterization of the PSMA-Targeted Hybrid Tracer PSMA-I&F for Nuclear and Fluorescence Imaging of Prostate Cancer. *J Nucl Med* **2019**;60:71-8.
24. Hell SW, Wichmann J. Breaking the diffraction resolution limit by stimulated emission: stimulated-emission-depletion fluorescence microscopy. *Opt Lett* **1994**;19:780-2.
25. Hell SW. Far-field optical nanoscopy. *Science* **2007**;316:1153-8.
26. Gorlitz F, Hoyer P, Falk HJ, Kastrup L, Engelhardt J, Hell SW. A STED Microscope Designed for Routine Biomedical Applications. *Prog Electromagn Res* **2014**;147:57-68.
27. Butkevich AN, Mitronova GY, Sidenstein SC, Klocke JL, Kamin D, Meineke DN*, et al.* Fluorescent Rhodamines and Fluorogenic Carbopyronines for Super-Resolution STED Microscopy in Living Cells. *Angew Chem Int Ed Engl* **2016**;55:3290-4.
28. Hinner MJ, Johnsson K. How to obtain labeled proteins and what to do with them. *Curr Opin Biotechnol* **2010**;21:766-76.
29. Benesova M, Schafer M, Bauder-Wust U, Afshar-Oromieh A, Kratochwil C, Mier W*, et al.* Preclinical Evaluation of a Tailor-Made DOTA-Conjugated PSMA Inhibitor with Optimized Linker Moiety for Imaging and Endoradiotherapy of Prostate Cancer. *J Nucl Med* **2015**;56:914-20.

30. Baranski AC, Schafer M, Bauder-Wust U, Wacker A, Schmidt J, Liolios C*, et al.* Improving the Imaging Contrast of (68)Ga-PSMA-11 by Targeted Linker Design: Charged Spacer Moieties Enhance the Pharmacokinetic Properties. *Bioconjug Chem* **2017**;28:2485-92.
31. Gorges TM, Riethdorf S, von Ahsen O, Nastal YP, Rock K, Boede M*, et al.* Heterogeneous PSMA expression on circulating tumor cells: a potential basis for stratification and monitoring of PSMA-directed therapies in prostate cancer. *Oncotarget* **2016**;7:34930-41.
32. Dunn KW, Kamocka MM, McDonald JH. A practical guide to evaluating colocalization in biological microscopy. *Am J Physiol Cell Physiol* **2011**;300:C723-42.
33. Pastan IH, Willingham MC. Receptor-mediated endocytosis of hormones in cultured cells. *Annu Rev Physiol* **1981**;43:239-50.
34. Mellman I. Endocytosis and molecular sorting. *Annu Rev Cell Dev Biol* **1996**;12:575-625.
35. Bertelsen V, Sak MM, Breen K, Rodland MS, Johannessen LE, Traub LM*, et al.* A chimeric pre-ubiquitinated EGF receptor is constitutively endocytosed in a clathrin-dependent, but kinase-independent manner. *Traffic* **2011**;12:507-20.
36. Miller SE, Mathiasen S, Bright NA, Pierre F, Kelly BT, Kladt N*, et al.* CALM regulates clathrin-coated vesicle size and maturation by directly sensing and driving membrane curvature. *Developmental cell* **2015**;33:163-75.
37. Demandolx D, Davoust J. Multicolour analysis and local image correlation in confocal microscopy. *J Microsc-Oxford* **1997**;185:21-36.
38. Banerjee SR, Pullambhatla M, Byun Y, Nimmagadda S, Foss CA, Green G*, et al.* Sequential SPECT and optical imaging of experimental models of prostate cancer with a dual modality inhibitor of the prostate-specific membrane antigen. *Angewandte Chemie* **2011**;50:9167-70.
39. Gottfert F, Wurm CA, Mueller V, Berning S, Cordes VC, Honigmann A*, et al.* Coaligned dual-channel STED nanoscopy and molecular diffusion analysis at 20 nm resolution. *Biophys J* **2013**;105:L01-3.
40. Hotta J, Fron E, Dedecker P, Janssen KP, Li C, Mullen K*, et al.* Spectroscopic rationale for efficient stimulated-emission depletion microscopy fluorophores. *J Am Chem Soc* **2010**;132:5021-3.
41. Perico ME, Grasso S, Brunelli M, Martignoni G, Munari E, Moiso E*, et al.* Prostate-specific membrane antigen (PSMA) assembles a macromolecular complex regulating growth and survival of prostate cancer cells "in vitro" and correlating with progression "in vivo". *Oncotarget* **2016**;7:74189-202.
42. Schmidt S, Gericke B, Fracasso G, Ramarli D, Colombatti M, Naim HY. Discriminatory Role of Detergent-Resistant Membranes in the Dimerization and Endocytosis of Prostate-Specific Membrane Antigen. *PLoS One* **2013**;8:e66193.
43. Colombatti M, Grasso S, Porzia A, Fracasso G, Scupoli MT, Cingarlini S*, et al.* The prostate specific membrane antigen regulates the expression of IL-6 and CCL5 in prostate tumour cells by activating the MAPK pathways. *PLoS One* **2009**;4:e4608.

## Figure Legends

**Fig. 1. Chemical structure and basic *in cellulo* characterization of STED-compatible dual-labeled PSMA inhibitors.** (**A**) The conjugates consist of the PSMA binding motif “Glu-urea-Lys” (orange), the radiometal chelator “HBED-CC” (gray) and the fluorescence moiety “STAR RED” (red) or “STAR 635P” (blue) conjugated via $PEG_2$ linker (black). (**B**) Confocal images of LNCaP and 22Rv1 cells after incubation with 50 nM (LNCaP) and 250 nM (22Rv1) Glu-urea-Lys-HBED-CC-STAR RED for 15 min (LNCaP) and 45 min (22Rv1). Scale bars, 10 µm. (**C**) Frequency and (**D**) duration of cell division of untreated (LNCaP, green: experiments *N*=13, divisions *N*=347; 22Rv1, pale green: experiments *N*=6, divisions *N*=1029) and treated (100 nM Glu-urea-Lys-HBED-CC-STAR RED, LNCaP, red: experiments *N*=16, divisions *N*=624; 22Rv1, pale red: experiments *N*= 5, divisions *N*=1029 / 100 nM Glu-urea-Lys-HBED-CC-STAR 635P, LNCaP, blue: experiments *N*=14, divisions *N*=408; 22Rv1, pale blue: experiments *N*=5, divisions *N*=940) cells assessed by holographic time-lapse cytometry. Box plot indicates the interquartile range (box), the outer-most data points falling within 1.5× interquartile range (whiskers), the median (center line) and the mean (triangle). Significance: * $p<0.5$, ** $p<0.05$, *** $p<0.005$. The results are summarized in Table S3.

**Fig. 2. Organ distribution and small-animal PET imaging study of $^{68}$Ga-labeled STED-compatible dual-labeled PSMA inhibitors.** (**A**) Organ distribution and corresponding tumor-to-organ (T/O) ratios of 60 pmol [$^{68}$Ga]Ga-Glu-urea-Lys-HBED-CC-STAR RED (red) and [$^{68}$Ga]Ga-Glu-urea-Lys-HBED-CC-STAR 635P (blue) at 1 h p.i.. Data are expressed as mean ± SD (*N*=3). The results are summarized in Table S4. (**B**) From left to right: Confocal images of 5 nmol [$^{68}$Ga]Ga-Glu-urea-Lys-HBED-

CC-STAR RED (red) and DAPI (blue) in tumor tissue cryosections at 1 h p.i. and of 5 nmol [$^{68}$Ga]Ga-Glu-urea-Lys-HBED-CC-STAR RED (red) and autofluorescence (green) in muscle tissue cryosections at 1 h p.i.. Scale bar, 10 µm. (**C**) Whole-body maximum intensity projections of 0.5 nmol [$^{68}$Ga]Ga-Glu-urea-Lys-HBED-CC-STAR RED (~50 MBq) in LNCaP- (left) and PC-3- (right) tumor-bearing athymic nude mice (right trunk) 120 min p.i. obtained from small animal PET imaging. (**D**) Corresponding time activity curves for tumor and muscle (left) and for other organs (right). SUV=standardized uptake value.

**Fig. 3. STED imaging of Glu-urea-Lys-HBED-CC-STAR RED after PSMA binding and clathrin-mediated endocytosis.** (**A**) Overview confocal (bottom) and STED (top) image of LNCaP cells after incubation with 100 nM PSMA inhibitor for 45 min. STED imaging resolves a heterogeneous distribution of PSMA inhibitor bound PSMA with areas of higher and lower PSMA density. Marked membrane regions (dotted cyan lines) in the overview are shown as magnified STED close-ups on the right. Scale bar overview, 5 µm; scale bar close-ups, 2 µm. (**B**) Cytoplasmic vesicle shown in confocal (top) and STED (bottom) mode exemplifying the resolution improvement of STED. White arrows indicate the direction of line profiles (drawn on raw data) depicted in (**C**) of the STED (orange) and confocal (gray) data. Pixel size is 20 nm for both confocal and STED image. Scale bar, 250 nm. (**D**) Confocal image (left) of a LNCaP cell after incubation with 100 nM PSMA inhibitor for 1 h at 37°C showing different vesicle densities in the cytoplasm with accumulation favorably in filopodia. The marked vesicles are depicted as STED close-ups on the right. Scale bar cell, 10 µm; scale bar vesicles, 250 nm. (**E**) To prove clathrin-mediated endocytosis, colocalization between SNAP-tagged CLC labeled with 610CP (gray) and PSMA

779 inhibitor (red) was analyzed as illustrated in the sketch (top, ex – extracellular, cyto –
780 cytoplasm). Exemplary dual color live cell confocal image (bottom) of a CCV after
781 incubation with 50 nM PSMA inhibitor for 15 min. Scale bar, 500 nm. (**F**) Pearson's
782 correlation coefficient between SNAP-tagged CLC and PSMA inhibitor. Data are
783 expressed as mean ± SD (10 min *N*=7, 15 min *N*=14). Significance: *** p<0.005. The
784 results are summarized in Table S6. (**G**) Size distribution of endoplasmic vesicles in
785 LNCaP (left) and 22Rv1 (right) cells after 30/45/60 min of internalization time with
786 100 nM PSMA inhibitor (ns – no significant differences). The fluorescence signal of
787 individual vesicles was fitted with a two-dimensional ring function (LNCaP: 30 min
788 *N*=50, 45 min *N*=50, 60 min *N*=50; 22Rv1: 30 min *N*=81, 45 min *N*=38, 60 min *N*=59).
789 Box plot indicates the interquartile range (box), the outer-most data points falling
790 within 1.5× interquartile range (whiskers), the median (center line) and the mean
791 (triangle). The results are summarized in Table S7. All STED data shown are
792 background corrected and linearly deconvolved. Fig. S7 illustrates the post
793 processing steps from raw data to background corrected and linearly deconvolved
794 data. All confocal data shown are raw data except for (**E**).

795

796 **Fig. 4. Intracellular fate of the PSMA/PSMA inhibitor complex.** (**A**) Sketch of the
797 novel dual-staining approach targeting PSMA with indirect IF and PSMA inhibitor (ex
798 – extracellular, cyto – cytoplasm). (**B**) Definition of fluorogram sections (for details
799 see text). (**C**) Exemplary fluorograms (top) and corresponding STED images (bottom)
800 of LNCaP cells STAR 600-immunolabeled for PSMA (cyan) and co-incubated with
801 100 nM Glu-urea-Lys-HBED-CC-STAR RED (red) for different internalization times.
802 All scale bars, 5 µm. (**D**) Exemplary STED images of cytoplasmic vesicles in LNCaP
803 (top) and 22Rv1 (bottom) cells. After internalization, PSMA (cyan) and PSMA

804 inhibitor (red) first colocalize at the vesicle membrane (left). Within the first hour of
805 internalization, the PSMA/PSMA inhibitor complex segregates and the inhibitor
806 initially distributes homogeneously in the vesicles (right). Scale bar, 250 nm. (**E**)
807 Exemplary confocal images of LNCaP (top) and 22Rv1 (bottom) cells after 30 min
808 (left) and after 6 h of internalization of 100 nM Glu-urea-Lys-HBED-CC-STAR RED
809 (right) showing that the PSMA inhibitor eventually disperses in the cytoplasm. Scale
810 bar, 5 µm. (**F**) Quantification of the extracellular (gray) and cytoplasmic ((pale)
811 orange) background of STED images of LNCaP cells (top) and of confocal images of
812 22Rv1 cells (bottom) after 30 min and after 6 h of incubation with 100 nM Glu-urea-
813 Lys-HBED-CC-STAR RED (LNCaP: ex 30 min *N*=32, cyto 30 min *N*=32, ex 6 h
814 *N*=48, cyto 6 h *N*=48; 22Rv1: ex 30 min *N*=48, cyto 30 min *N*=48, ex 6 h *N*=88, cyto
815 6 h *N*=88). Box plot indicates the interquartile range (box), the outer-most data points
816 falling within 1.5× interquartile range (whiskers), the median (center line) and the
817 mean (triangle). Significance: *** $p<0.005$. The results are summarized in Table S8.
818 All STED data shown are background corrected and linearly deconvolved. All
819 confocal data shown are raw data.

820

821 **Fig. 5. Endosomal recycling of PSMA after pH dependent PSMA/PSMA inhibitor**
822 **complex segregation.** (**A**) Exemplary confocal images (top) of living LNCaP (left)
823 and 22Rv1 (right) cells STAR 600-immunolabeled for PSMA (cyan) and incubated
824 with 500 nM LysoTracker™ Green DND-26 (magenta) after >20 h internalization
825 time. Marked endosomes (white arrows) are depicted as close-ups (bottom) with
826 PSMA shown in STED mode and the STED-incompatible LysoTracker in confocal
827 mode. Exemplary LNCaP movie is supplied (Movie S5). Scale bar overview, 5 µm;
828 scale bar close-ups, 500 nm. (**B**) Pearson's correlation coefficient between

immunolabeled PSMA and LysoTracker™ Green DND-26 in living LNCaP and 22Rv1 cells. Data are expressed as mean ± SD (LNCaP 1 h *N*=21, +20 h *N*=26; 22Rv1 1 h *N*=39, +20 h *N*=81). Significance: *** p<0.005. The results are summarized in Table S9. (**C**) Exemplary STED image of a LNCaP cell (left) and exemplary confocal image of a 22Rv1 cell (right) STAR 600-immunolabeled for PSMA (cyan) and incubated with 100 nM Glu-urea-Lys-HBED-CC-STAR RED (red) for 1 h (LNCaP) and 6 h (22Rv1) of internalization time. Marked regions (dotted yellow line) are depicted as STED close-ups showing recycled PSMA at the cell membrane. Scale bar cell, 5 µm; scale bar close-ups, 2 µm. (**D**) Quantification of pH dependence of PSMA binding of the primary and secondary antibody (either STAR RED- or STAR 600-labeled) complex, Glu-urea-Lys-HBED-CC-STAR RED and -STAR 635P to LNCaP cells by flow cytometry. Binding percentage was calculated based on normalizing binding to 100% at pH 7.0. Data are expressed as mean ± SD (*N*=3). Significance: ** p<0.05, *** p<0.005. The results are summarized in Table S10. All STED data shown are background corrected and linearly deconvolved. All confocal data shown are background corrected. The LysoTracker™ Green DND-26 confocal data of the 22Rv1 close-ups in (**A**) are additionally smoothed with a Gaussian low pass filter with a width of one pixel.

Fig. 1

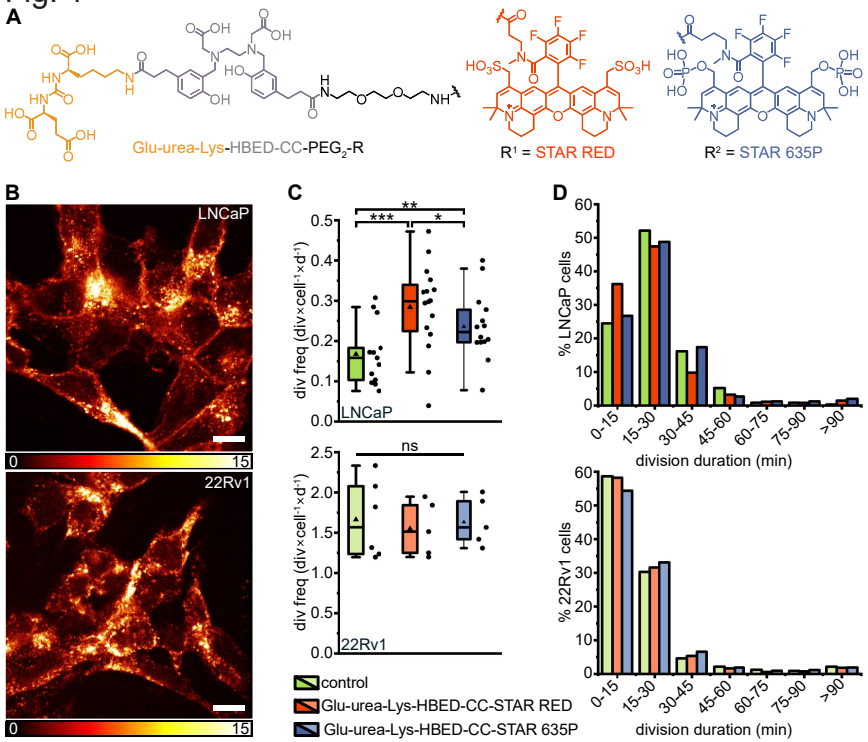
A
Glu-urea-Lys-HBED-CC-PEG2-R
R1 = STAR RED
R2 = STAR 635P
B
LNCaP
0
15
22Rv1
0
15
C
div freq (div×cell-1×d-1)
LNCaP
22Rv1
ns
control
Glu-urea-Lys-HBED-CC-STAR RED
Glu-urea-Lys-HBED-CC-STAR 635P
D
% LNCaP cells
% 22Rv1 cells
0-15
15-30
30-45
45-60
60-75
75-90
>90
division duration (min)

Fig. 2

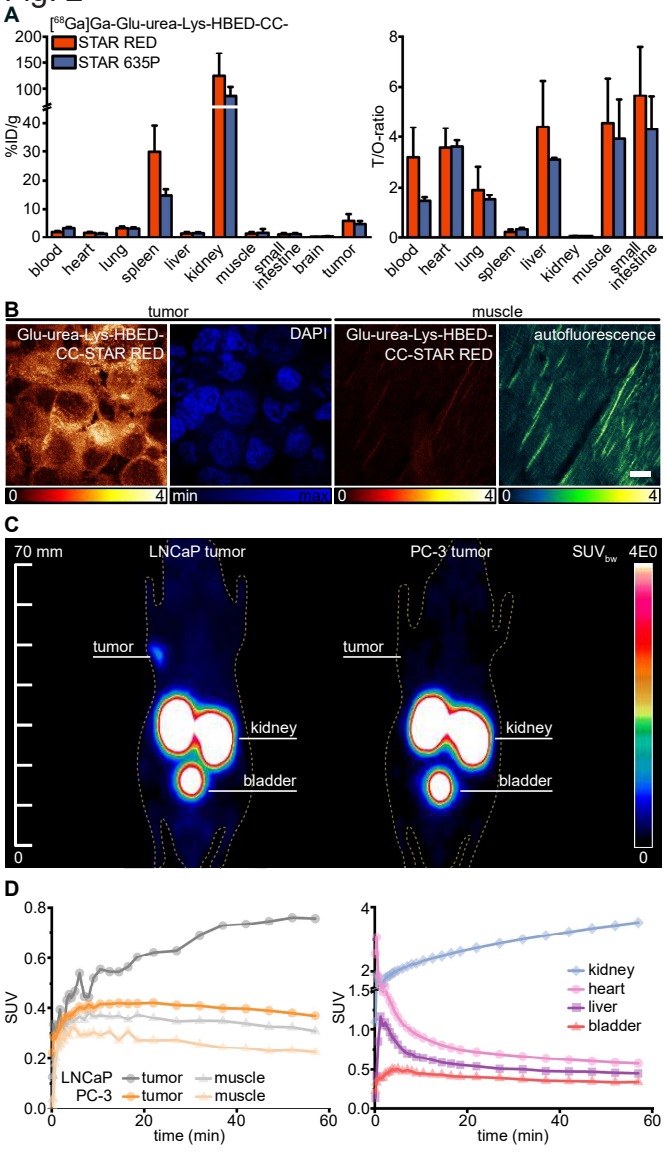
A
[68Ga]Ga-Glu-urea-Lys-HBED-CC-
STAR RED
STAR 635P
%ID/g
T/O-ratio
blood
heart
lung
spleen
liver
kidney
muscle
small intestine
brain
tumor
B
tumor
muscle
Glu-urea-Lys-HBED-CC-STAR RED
DAPI
autofluorescence
min
max
C
70 mm
LNCaP tumor
PC-3 tumor
SUVbw
4E0
tumor
kidney
bladder
D
SUV
LNCaP tumor
LNCaP muscle
PC-3 tumor
PC-3 muscle
kidney
heart
liver
bladder
time (min)

Fig. 3

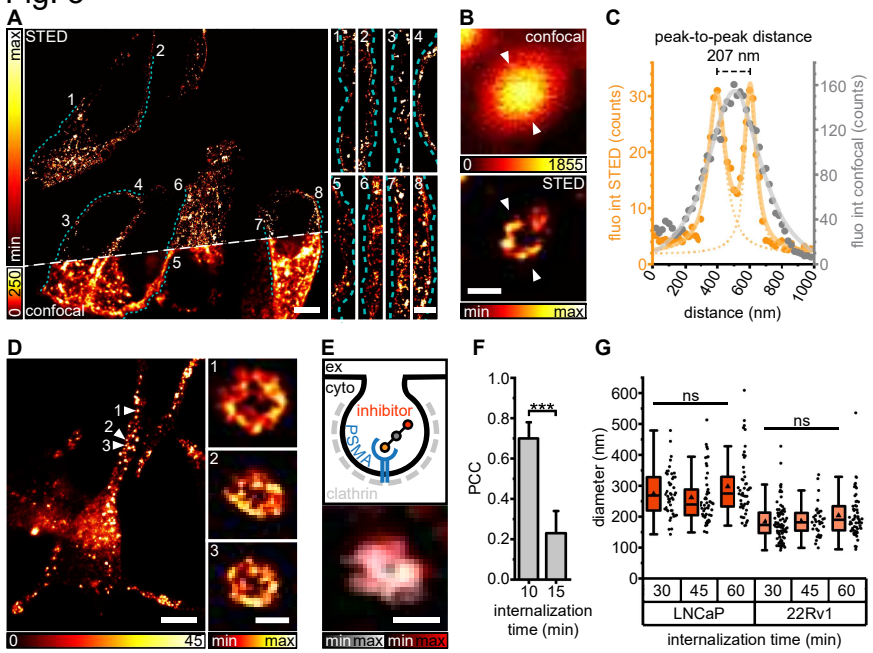
A
STED
max
min
0
250
confocal
1
2
3
4
5
6
7
8
B
confocal
0
1855
STED
min
max
C
peak-to-peak distance
207 nm
fluo int STED (counts)
fluo int confocal (counts)
distance (nm)
D
0
45
min
max
E
ex
cyto
inhibitor
PSMA
clathrin
min max min max
F
PCC
***
10
15
internalization
time (min)
G
diameter (nm)
ns
ns
30
45
60
30
45
60
LNCaP
22Rv1
internalization time (min)

Fig. 4

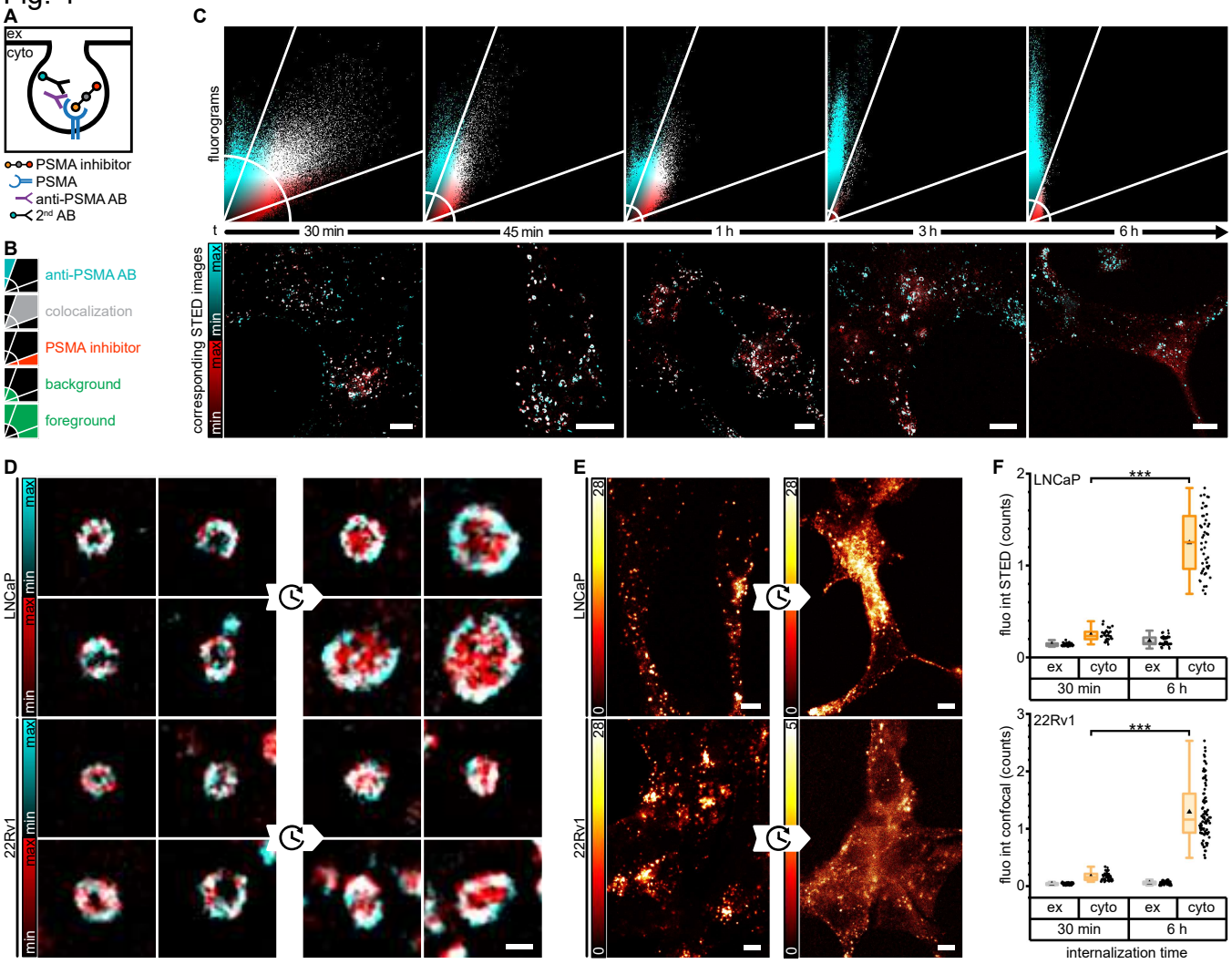
A
ex
cyto
PSMA inhibitor
PSMA
anti-PSMA AB
2nd AB
B
anti-PSMA AB
colocalization
PSMA inhibitor
background
foreground
C
fluorograms
t
30 min
45 min
1 h
3 h
6 h
corresponding STED images
max
min
max
min
D
LNCaP
22Rv1
max
min
max
min
max
min
max
min
E
LNCaP
22Rv1
28
0
28
0
28
0
5
0
F
LNCaP
***
fluo int STED (counts)
2
1
0
ex
cyto
ex
cyto
30 min
6 h
22Rv1
***
fluo int confocal (counts)
3
2
1
0
ex
cyto
ex
cyto
30 min
6 h
internalization time

Fig. 5

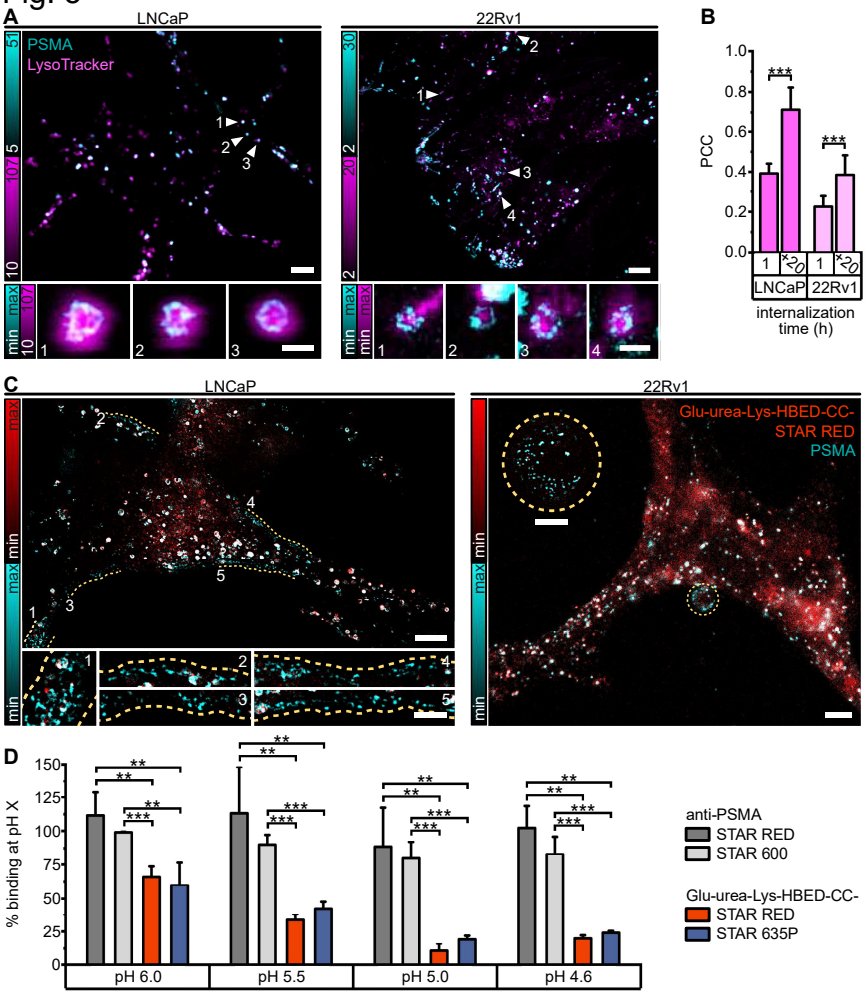
A
LNCaP
22Rv1
PSMA
LysoTracker
B
PCC
internalization time (h)
LNCaP
22Rv1
C
LNCaP
22Rv1
Glu-urea-Lys-HBED-CC-STAR RED
PSMA
D
% binding at pH X
pH 6.0
pH 5.5
pH 5.0
pH 4.6
anti-PSMA
STAR RED
STAR 600
Glu-urea-Lys-HBED-CC-
STAR RED
STAR 635P